SUPPORTING INFORMATION

Ultrafast Irreversible Phototautomerization of *ortho*-Nitrobenzaldehyde

Annapaola Migani,[‡] Verónica Leyva,[#] Ferran Feixas,[‡] Thomas Schmierer,[§] Peter Gilch,[§] Inés Corral,[#] Leticia González,[#] Lluís Blancafort[‡]

[‡]*Insititute of Computational Chemistry and Department of Chemistry, University of Girona, Campus de Montilivi, 17071 Girona, Spain*

[#]*Institut für Physikalische Chemie, Friedrich-Schiller-Universität Jena, Helmholtzweg 4, 07743 Jena, Germany*

[§]*Institut für Physikalische Chemie, Heinrich Heine Universität Düsseldorf, Universitätsstr. 1, 40225 Düsseldorf, Germany.*

o-NBA Phototautomerization– Supporting Information - Migani et al.

TABLE OF CONTENTS Page

Experimental Details SI3

Computational Details SI3

References SI6

Table SI1. Vertical excitation energies and oscillator strenghts SI7

Table SI2. CASSCF/6-31G* and MS-CASPT2/ ANO-L energies for critical points SI8

Figure SI1. Molecular orbitals for (14,12) active space SI9

Figure SI2. Molecular orbitals for (16,13) active space SI9

Figure SI3. FC → $(n,\pi^*)_{Min}$ MS-CASPT2 LIIC SI10

Figure SI4. S_1 excited state MEP **$(n,\pi^*)_{Min}$** → S_1 (n,π^*) TS → **$(S_1/S_0)_{X\text{-}HT}$** SI11

Figure SI5. S_0 state MEP **$(S_1/S_0)_{X\text{-}HT}$ → *anti*-Ket** SI12

Figure SI6. FC → $(\pi,\pi^*)_{Min}$ → $(S_3/S_2)_X$ MS-CASPT2 LIIC SI13

Figure SI7. S_2 excited state MEP **$(S_3/S_2)_X$ → $(S_2/S_1)_X$** SI14

Figure SI8. S_1 excited state MEP **$(S_1/S_0)_{X\text{-}HT}$ → $(S_2/S_1)_X$ → $(S_1/S_0)_{X\text{-}Ket}$** SI15

Figure SI9. S_0 state MEP **$(S_1/S_0)_{X\text{-}Ket}$ → *anti*-Ket** SI16

Figure SI10. S_0 state MEP **FC → *anti*-Ket** SI17

Figure SI11. FC geometry SI18

Figure SI12. $(\pi,\pi^*)_{Min}$ geometry, relevant molecular orbitals (MO) SI18

Figure SI13. $(S_3/S_2)_X$ MECI geometry, branching space vectors, relevant MO SI19

Figure SI14. $(S_2/S_1)_X$ MECI geometry, branching space vectors, relevant MO SI20

Figure SI15. $(S_1/S_0)_{X\text{-}Ket}$ MECI geometry, branching space vectors, relevant MO SI21

Figure SI16. *syn*-Ket and ***anti*-Ket** geometries, relevant MO SI22

Figure SI17. $(S_1/S_0)_{X\text{-}HT}$ MECI geometry, branching space vectors, relevant MO SI23

Figure SI18. $(n,\pi^*)_{Min}$ geometry, relevant MO SI24

Figure SI19. Bir geometry, relevant MO SI24

Figure SI20. TS geometry, imaginary frequency SI25

Cartesian coordinates of optimized structures SI26

o-NBA Phototautomerization– Supporting Information - Migani et al.

Experimental Details

Transient absorption data depicted in Figure 1 were recorded with the set-up for FSRS described in Ref. [1] without using the Raman pump branch. Absorption changes were probed by a white-light continuum generated in CaF_2. This probe light was focused to a size of 40 μm (full width at half maximum, FWHM) at the sample location. Data were recorded for two different excitation wavelengths, namely 258 and 388nm. These wavelengths were obtained by frequency doubling and tripling of the fundamental of a Ti:sapphire laser amplifier system (Clark CPA 2001, repetition rate of 1 kHz). Beam diameters of the excitation light at the sample location amounted to 85 μm. For the measurement with excitation at 388nm the solution of *o*-NBA in tetrahydrofuran (THF) had a concentration of ~48mM. Such high concentrations were necessary since the wavelength of 388nm is at the very edge of the *o*-NBA absorption.[2] Measurements with different excitation energies ensured that no two-photon absorption occurs for the finally chosen energy of 210nJ. The excitation energy in the 258nm experiment amounted to 300nJ. The sample solution had a concentration of 19mM. For either excitation wavelengths, the sample solution was guided through the focal region by a wire guided jet system. THF and *o*-NBA were purchased from Merck (Germany) and used as received. The temporal resolution of the experiment is limited by the durations of the excitation pulses and is approximately 200 fs.

Computational Details

The computational results are obtained with the MS-CASPT2//CASSCF approach (multistate second order multiconfigurational perturbation energies on the complete active space self-consistent field optimized structures and minimum energy paths). The MS-CASPT2 calculationsare carried out with a CAS(16,13)/ANO-L reference wave function. The (16,13) active space provides a balanced description of all relevant valence states. All structures have been optimized at the CASSCF/6-31G* level except for the minimum of the (π,π^*) state accessed at 258 nm, where the CASSCF optimization has not been possible because of the high density of states. Thus, $\mathbf{(\pi,\pi^*)_{Min}}$ (Figure 4 below) has been optimized with time dependent density functional theory (DFT), and the paths from the Franck-Condon structure (**FC**) to $\mathbf{(\pi,\pi^*)_{Min}}$ and $\mathbf{(\pi,\pi^*)_{Min}}$ to $\mathbf{(S_3/S_2)_X}$ have been approximated by linear interpolations in internal coordinates (LIIC). For a similar reason, the path from **FC** to $\mathbf{(n,\pi^*)_{Min}}$ is also approximated with a

LIIC. All other paths have been optimized as intrinsic reaction coordinates on the relevant state. The calculations have been carried out with the Gaussian[3] and Molcas[4] programs, and the Computational Details are given in the SI.

The calculations were performed using a MS-CASPT2/ANO-L//CASSCF/6-31G* protocol (multistate second order perturbation energies on the complete active space self-consistent field optimized structures and minimum energy paths). Geometry optimizations (minima, transition states, conical intersections) and minimum energy paths (MEP) were carried out at the multi-configurational CASSCF level with a (14,12) active space, unless specified below, including eight π orbitals and four in-plane σ/n orbitals (Figure SI1), and the 6-31G*[5] one-electron basis set in all atoms. The Franck-Condon minimum (**FC**) was optimized with a (12,11) active space including the complete set of eleven π orbitals. Transition structures and minima have been characterized by numerical frequency calculations. The number of state-averaged roots included in each optimization and MEP calculation was varied as required (cfr. Table SI2, and Figures SI4-6, SI8-9). The MEPs were constructed combining the initial relaxation direction (IRD) and intrinsic reaction coordinate (IRC) procedures, as detailed elsewhere.[6] The MEPs from conical intersections have been started at the CASSCF minimum energy conical intersection (MECI) geometry. Structures $\mathbf{(n,\pi^*)_{Min}}$, ***syn*-Ket** and **Bir** have been optimized with a C_s symmetry constraint.

In order to include the dynamic correlation and obtain the electronic energies, the MS-CASPT2 approach[7] was employed with an imaginary level-shift[8] correction of 0.1 au and no IPEA[9] correction. In the MS-CASPT2 calculations the active space of the CASSCF reference wavefunction was enlarged to (16,13) including all valence orbitals except the doubly occupied nodeless NO_2 group π orbital (Figure SI2), and the number of roots computed with equal weights in the CASSCF reference wavefunction calculation was fourteen. The basis set was improved to ANO-L[10] type contracted to 4s3p1d for C,O, and N, and to 3s2p for H. Compared to our previous study,[2] the MS-CASPT2/14-root state-average CASSCF(16,13) level of theory allows for the *simultaneous* description with the same accuracy of the (n,π^*) and (π,π^*) excited states. The calculated vertical excitations (Table SI1) are in good agreement with our previous study.[2]

o-NBA Phototautomerization– Supporting Information - Migani et al.

All geometry optimizations and MEP calculations were performed with the Gaussian-03[3] program while MS-CASPT2 calculations were carried out with the MOLCAS-7.0[4] program. The photochemical reaction paths in Figures 3, 4, and 5 are constructed by merging the following data: *ESHT on the (n,π*) state (Figure 3)*: linear interpolation in internal coordinates (LIIC) from **FC** to $\mathbf{(n,\pi^*)_{Min}}$ (Figure SI3), MEP from $\mathbf{(n,\pi^*)_{Min}}$ to $\mathbf{(S_1/S_0)_{X\text{-}HT}}$ (Figure SI4), and MEP from $\mathbf{(S_1/S_0)_{X\text{-}HT}}$ to ***anti*-Ket** (Figure SI5). *Decay of the (π,π*) state (Figure 4):* LIIC from **FC** to $\mathbf{(\pi,\pi^*)_{Min}}$ (Figure SI6). *CI cascade (Figure 5)*: MEP from $\mathbf{(S_3/S_2)_X}$ to $\mathbf{(S_2/S_1)_X}$ (Figure SI7), MEP from $\mathbf{(S_2/S_1)_X}$ to $\mathbf{(S_1/S_0)_{X\text{-}Ket}}$ (Figure SI8), and MEP from $\mathbf{(S_1/S_0)_{X\text{-}Ket}}$ to ***anti*-Ket** (Figure SI9). All energies are given in eV with respect to **FC**. In Figures SI3 – SI9, the relevant states are characterized as aldehyde ground state (configuration $n^2\pi^{*0}$), ketene ground state (configuration $n^2\pi^{*0}$), (π,π^*) and (n,π^*). For the (n,π^*) states, the excitation comes from the oxygen lone pairs on the aldehyde or nitro groups, or their combination. The character of these orbitals is given in Figures SI11 – SI19.

With MS-CASPT2 the energy separation between intersecting electronic states at the CASSCF MECI geometries can increase up to approximately 0.8 eV. However, points of degeneracy at the MS-CASPT2 level (energy gap < 0.1 eV) could be located along the computed MEPs at nuclear configurations slightly displaced from the CASSCF MECI geometries. These points are marked with blue arrows in Figures SI4b ($\mathbf{(S_1/S_0)_{X\text{-}HT}}$), SI7b ($\mathbf{(S_3/S_2)_X}$), SI8b ($\mathbf{(S_2/S_1)_X}$), and SI9b ($\mathbf{(S_1/S_0)_{X\text{-}Ket}}$). The conical intersection energies given in Figures 3 and 4 in the manuscript correspond to these structures.

For $\mathbf{(n,\pi^*)_{Min}}$, the CASSCF optimization of the state that correlates with S_2 at **FC** (excitation from the oxygen lone pair of the nitro group) yields a non-planar structure on S_1. However, the symmetry constrained C_s minimum of that state is lower in energy at the MS-CASPT2 level, and this is the structure given in Figures 3 and SI17. The reaction path from **FC** is approximated by a linear interpolation in internal coordinates (LIIC) (see Figure SI3).

The optically active (π,π^*) state is computed as the eleventh root in the 14-root state average CASSCF(16,13) reference wavefunction calculation, which prevents the CASSCF optimization of the corresponding excited-state minimum. Therefore, the (π,π^*) excited-state relaxed geometry, $\mathbf{(\pi,\pi^*)_{Min}}$ (Figure SI12), was obtained by means of a TDDFT optimization (6-311G** basis set[5] and hybrid PBE0[11] density functional)

subject to a planar symmetry constraint. The reaction paths from **FC** to $(\pi,\pi^*)_{Min}$ and from $(\pi,\pi^*)_{Min}$ to $(S_3/S_2)_X$ are approximated by LIIC calculations (see Figure SI6).

The differences between our results for path 1 (almost barrierless ESHT leading directly to the ground state product, see Figure 3 in the main text) and a recent DFT based study, which claims that the ketene product is formed on S_1 and the ESHT has a considerable barrier,[12] are due to the approach used to obtain the energy profile. In Ref. 3, the path was optimized for the ground state and the excited state energy was computed along that coordinate. This approach can be misleading when the ground and excited state coordinates are different, as in the present case. In our approach, we obtain the proper mechanistic picture by optimizing the excited state coordinate directly.

References

[1] S. Laimgruber, H. Schachenmayr, B. Schmidt, W. Zinth, P. Gilch, *Appl. Phys. B* **2006**, *85*, 557-564.
[2] V. Leyva, I. Corral, T. Schmierer, B. Heinz, F. Feixas, A. Migani, L. Blancafort, P. Gilch, L. Gonzalez, *J. Phys. Chem. A* **2008**, *112*, 5046-5053.
[3] M. J. Frisch, G. W. Trucks, H. B. Schlegel, G. E. Scuseria, M. A. Robb, J. R. Cheeseman, J. A. Montgomery Jr., T. Vreven, K. N. Kudin, J. C. Burant, J. M. Millam, S. S. Iyengar, J. Tomasi, V. Barone, B. Mennucci, M. Cossi, G. Scalmani, N. Rega, G. A. Petersson, H. Nakatsuji, M. Hada, M. Ehara, K. Toyota, R. Fukuda, J. Hasegawa, M. Ishida, T. Nakajima, Y. Honda, O. Kitao, H. Nakai, M. Klene, X. Li, J. E. Knox, H. P. Hratchian, J. B. Cross, V. Bakken, C. Adamo, J. Jaramillo, R. Gomperts, R. E. Stratmann, O. Yazyev, A. J. Austin, R. Cammi, C. Pomelli, J. W. Ochterski, P. Y. Ayala, K. Morokuma, G. A. Voth, P. Salvador, J. J. Dannenberg, G. Zakrzewski, S. Dapprich, A. D. Daniels, M. C. Strain, O. Farkas, D. K. Malick, A. D. Rabuck, K. Raghavachari, J. B. Foresman, J. V. Ortiz, Q. Cui, A. G. Baboul, S. Clifford, J. Cioslowski, B. B. Stefanov, G. Liu, A. Liashenko, P. Piskorz, I. Komaromi, R. L. Martin, D. J. Fox, T. Keith, M. A. Al-Laham, C. Y. Peng, A. Nanayakkara, M. Challacombe, P. M. W. Gill, B. Johnson, W. Chen, M. W. Wong, C. Gonzalez, J. A. Pople, Gaussian 03, Revison C.01 ed., Gaussian, Inc., Pittsburgh, PA, **2003**.
[4] G. Karlström, R. Lindh, P. Å. Malmqvist, B. O. Roos, U. Ryde, V. Veryazov, P. O. Widmark, M. Cossi, B. Schimmelpfennig, P. Neograd y, L. Seijo, *Comput. Mater. Sci.* **2003**, *28*, 222-239.
[5] Harihara.Pc, J. A. Pople, *Theor. Chim. Acta* **1973**, *28*, 213-222.
[6] A. Migani, M. Olivucci, in *Conical Intersections: Electronic Structure, Dynamics and Spectroscopy, Vol. 15* (Eds.: W. Domcke, D. Yarkony, H. Köppel), World Scientific, **2004**.
[7] J. Finley, P. A. Malmqvist, B. O. Roos, L. Serrano-Andrés, *Chem. Phys. Lett.* **1998**, *288*, 299-306.
[8] N. Forsberg, P.-Å. Malmqvist, *Chem. Phys. Lett.* **1997**, *274*, 196.
[9] G. Ghigo, B. O. Roos, P. Å. Malmqvist, *Chem. Phys. Lett.* **2004**, *396*, 142-149.
[10] a) P. O. Widmark, B. Joakim, Persson, B. O. Roos, *Theor. Chim. Acta* **1991**, *79*, 419-432; b) P. O. Widmark, P. Å. Malmqvist, B. O. Roos, *Theor. Chim. Acta* **1990**, *77*, 291-306.
[11] C. Adamo, V. Barone, *J. Chem. Phys.* **1999**, *110*, 6158.
[12] S. Cheng, P. Song, S. Yang, H. Yin, K. Han, *Phys. Chem. Chem. Phys.* **2010**, *12*, 9067-9074.

Table SI1. Absolute and relative MS-CASPT2/CASSCF(16,13)/ANO-L vertical excitation energies and wave lengths, λ, of *o*-nitrobenzaldehyde, including electronic configuration and oscillator strength, *f*.

State	E [hartree]	ΔE [eV]	λ [nm]	Electronic configuration[a]	Squared CI coeff.	*f*
S_0	-548.82984	0.00		2222222200000	0.75	
S_1	-548.70467	3.40	364	22222u22d0000	0.27	0.001
(n,π^*)				22222u2200d00	0.18	
				2222222u00d00	0.06	
S_2	-548.69610	3.64	340	222222u2d0000	0.19	0.015
(n,π^*)				2222222ud0000	0.17	
				222u2222d0000	0.10	
				222222u200d00	0.07	
S_3	-548.68158	4.03	307	222u2222d0000	0.19	0.003
(π,π^*)				2222222u0000d	0.12	
				2222222u00d00	0.06	
S_4	-548.67311	4.26	291	2u222222d0000	0.35	0.002
(n,π^*)				2u22222200d00	0.14	
S_5	-548.66636	4.45	279	2222222ud0000	0.17	0.048
(π,π^*)				222222u2d0000	0.15	
				222222u200d00	0.09	

[a]Orbitals in Figure SI2.

Table SI2. Absolute CASSCF/6-31G* energies, and absolute and relative MS-CASPT2/CASSCF(16,13)/ANO-L energies with the corresponding electronic nature of relevant states, for the optimized critical points of *o*-nitrobenzaldehyde.

Structure	State	Active Space	E [hartree] CASSCF (14,12)	Configur-ation[a]	CI Coeff.	E [hartree] MS-CASPT2/ CASSCF (16,13)	ΔE [eV] MS-CASPT2/ CASSCF (16,13)
FC	S_0	(12,11)[b]	-547.04516	ald. gr. st.			
$(\pi,\pi^*)_{Min}$	S_0	-[c]		ald. gr. st.	0.73	-548.82605	0.10
	S_1			(n,π^*)	0.35	-548.72248	2.92
	S_2			(n,π^*)	0.37	-548.70351	3.44
	S_3			(n,π^*)	0.51	-548.68963	3.82
	S_4			(π,π^*)	0.45	-548.68751	3.87
	S_5			(π,π^*)	0.25	-548.68163	4.03
	S_6			ket. gr. st.	0.24	-548.61551	5.83
$(S_3/S_2)_X$	S_0	(14,12)[d]	-546.90713	ald. gr. st.	0.71	-548.76008	1.90
	S_1		-546.87996	(n,π^*)	0.69	-548.75373	2.07
	S_2		-546.81260	(n,π^*)	0.52	-548.70071	3.51
	S_3		-546.81223	ket. gr. st.	0.44	-548.67911	4.10
$(S_2/S_1)_X$	S_0	(14,12)[e]	-546.90160	(n,π^*)	0.79	-548.75749	1.97
	S_1		-546.85304	ald. gr. st./ ket. gr. st.	0.46/ 0.18	-548.70405	3.42
	S_2		-546.84986	ald. gr. st./ ket. gr. st.	0.28/ 0.29	-548.70282	3.46
$(S_1/S_0)_{X\text{-}Ket}$	S_0	(14,12)[f]	-546.91284	(n,π^*)		-548.75596	2.01
	S_1		-546.91273	ket. gr. st.		-548.74295	2.36
***syn*-Ket**	S_0	(14,12)[b]	-546.93784	ket. gr. st.	0.67	-548.76743	1.70
	S_1		-546.86170	(n,π^*)			
***anti*-Ket**	S_0	(14,12)[b]	-546.98265	ket. gr. st.	0.76	-548.79608	0.92
$(S_1/S_0)_{X\text{-}HT}$	S_0	(14,12)[f]	-546.89528	ald. gr. st.	0.76	-548.72597	2.83
	S_1		-546.89495	(n,π^*)	0.79	-548.75549	2.02
$(n,\pi^*)_{Min}$	S_0	(14,12)[f]	-546.99654	ald. gr. st.	0.60	-548.79957	0.82
	S_1		-546.92831	(n_{CO},π^*)	0.66	-548.71956	3.00
Bir	S_0	(14,12)[b]	-546.93508	(n_{CO},π^*)	0.80	-548.76736	1.70
TS	S_0	(14,12)[b]	-546.92669	ald. gr. st	0.68	-548.76775	1.69

[a]ald. gr. st.: aldehyde ground state; ket. gr. st.: ketene ground state. [b]Single-root optimization. [c]TD-DFT optimization. [d]Equally weighted four-root state-average optimization. [e]Equally weighted three- root state-average optimization. [f]Equally weighted two-root state-average optimization.

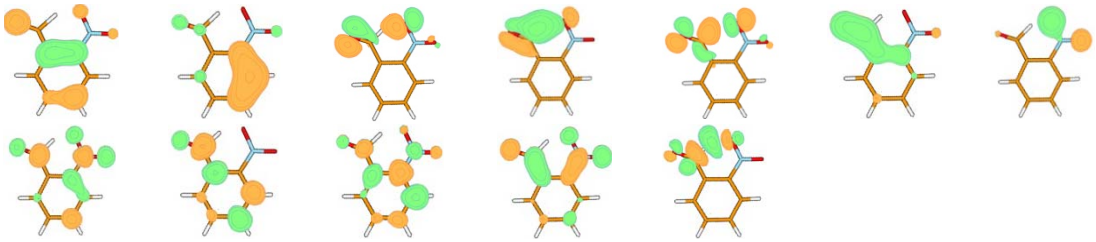

Figure SI1. Molecular orbitals included in the (14,12) active space of the CASSCF/6-31G* optimizations exemplified at the $\mathbf{(S_3/S_2)_X}$ geometry.

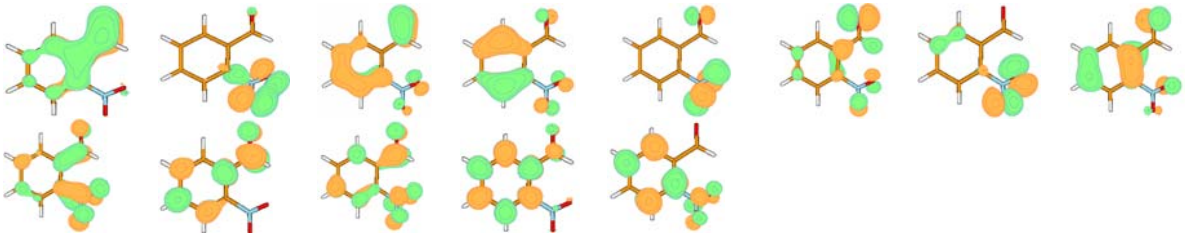

Figure SI2. Molecular orbitals included in the (16,13) active space of the CASSCF/ANO-L calculation state-averaged over 14 roots exemplified at the **FC** geometry.

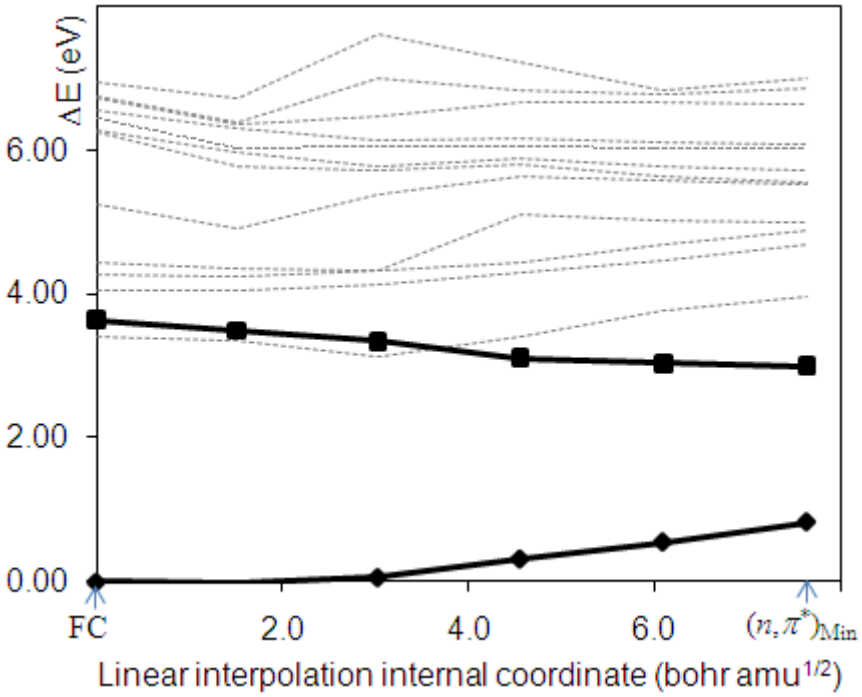

Figure SI3. Relative MS-CASPT2 energies along the LIIC from **FC** to $\boldsymbol{(n,\pi^*)_{Min}}$. (♦): aldehyde ground state; (■): (n,π^*); (--): other states.

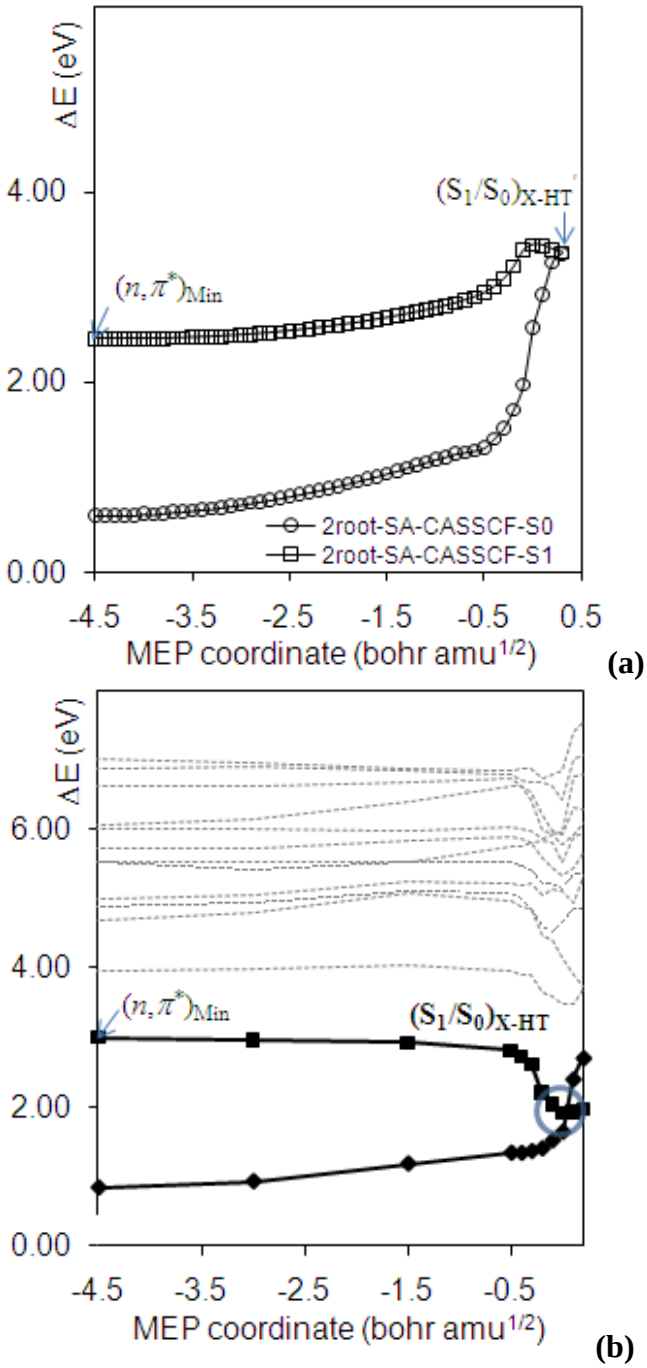

Figure SI4. (a) S_1 MEP from $\mathbf{(n,\pi^*)_{Min}}$ to $\mathbf{(S_1/S_0)_{X\text{-}HT}}$ composed by the CASSCF IRC calculations from the S_1 (n,π^*) transition state (0.0 au of the MEP coordinate) towards $\mathbf{(n,\pi^*)_{Min}}$ and $\mathbf{(S_1/S_0)_{X\text{-}HT}}$ (left and right directions, respectively). (b) MS-CASPT2 energy profiles along the $\mathbf{(n,\pi^*)_{Min}}$ to $\mathbf{(S_1/S_0)_{X\text{-}HT}}$ MEP. (♦): aldehyde ground state; (■): (n,π^*); (--): other states.

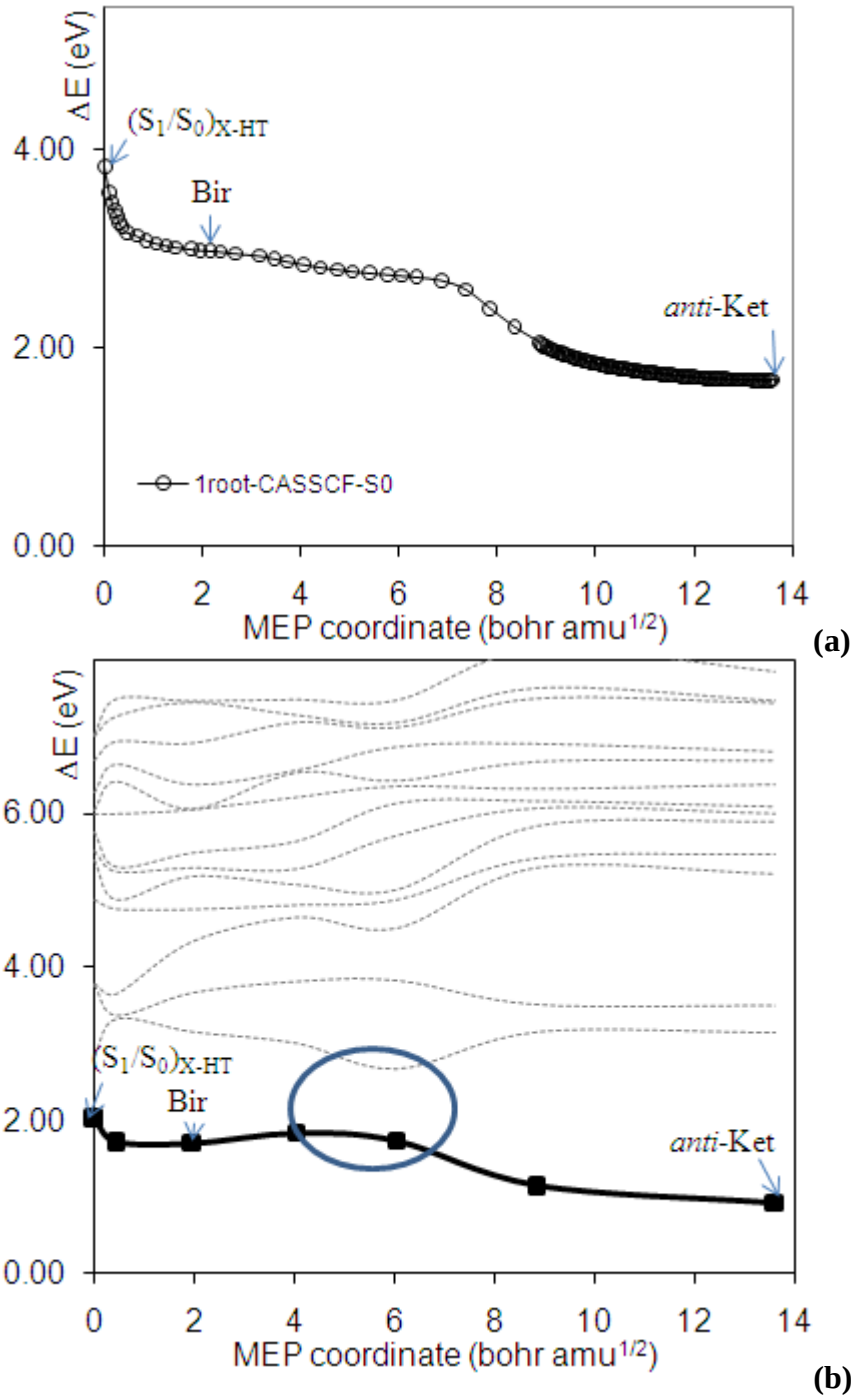

Figure SI5. (a) S_0 MEP from $\mathbf{(S_1/S_0)_{X\text{-}HT}}$ to ***anti*-Ket** through **Bir**, computed at the CASSCF level. (b) MS-CASPT2 energy profiles along the MEP from $\mathbf{(S_1/S_0)_{X\text{-}HT}}$ to ***anti*-Ket**. (■): S_0 (character changes from n_{CO},π^* to ketene, see main text); (--): other states. Blue circle: MS-CASPT2 transition state associated with an avoided crossing between the (n,π^*) and ketene states.

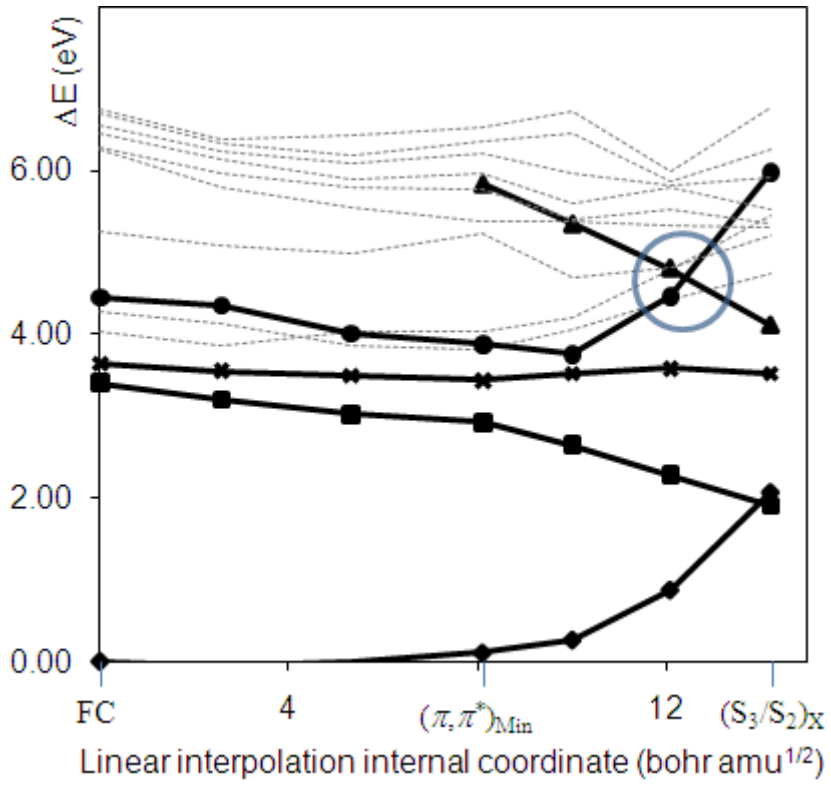

Figure SI6. Relative MS-CASPT2 energies along two combined LIIC calculations: **FC** to $(\pi,\pi^*)_{Min}$, and $(\pi,\pi^*)_{Min}$ to $(S_3/S_2)_X$. (♦): aldehyde ground state; (■): (n,π^*); (×): (n,π^*); (●): (π,π^*); (▲): ketene ground state; (--): other states.

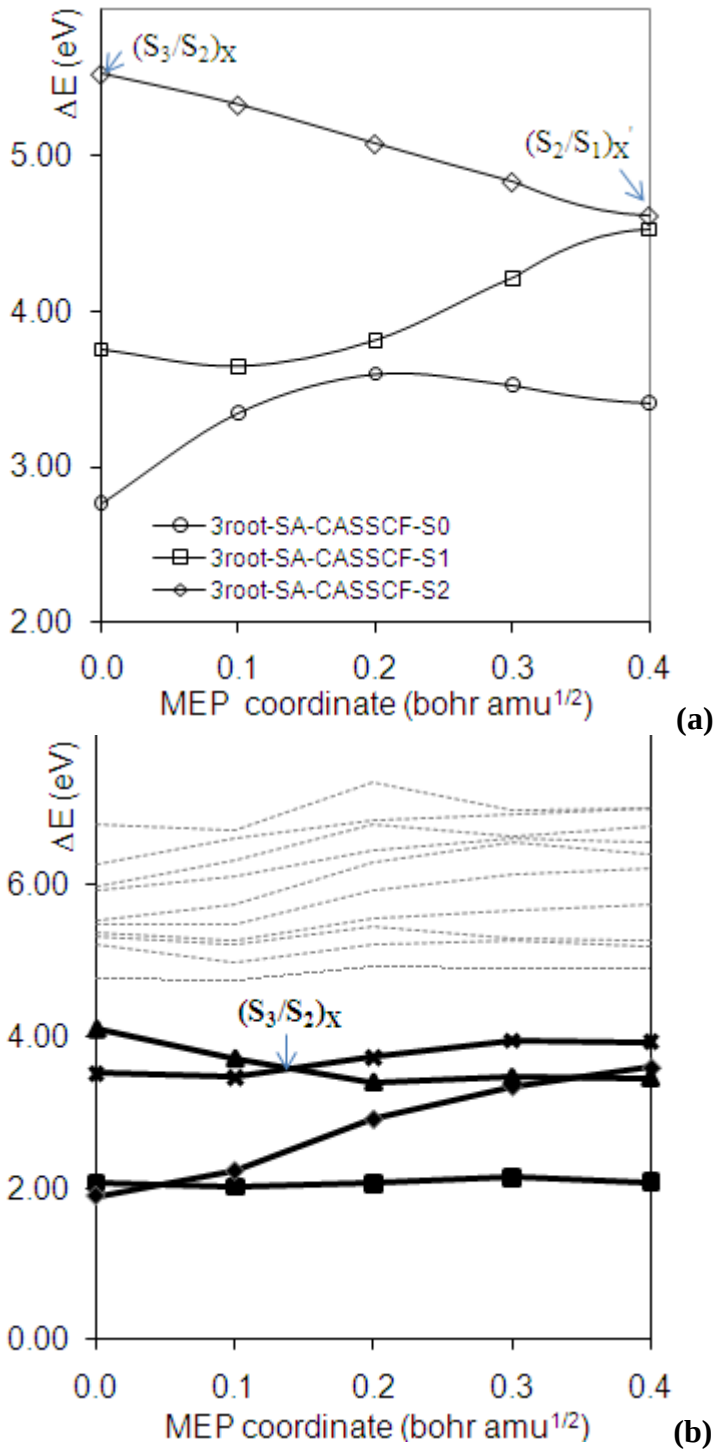

Figure SI7. (a) S_2 MEP from $\mathbf{(S_3/S_2)_X}$ to $\mathbf{(S_2/S_1)_X}$ computed at the CASSCF level. (b) MS-CASPT2 energy profiles along the $\mathbf{(S_3/S_2)_X}$ to $\mathbf{(S_2/S_1)_X}$ MEP. (♦): aldehyde ground state; (■): (n,π^*); (×): (n,π^*); (▲) ketene ground state; (--): other states.

o-NBA Phototautomerization– Supporting Information - Migani et al.

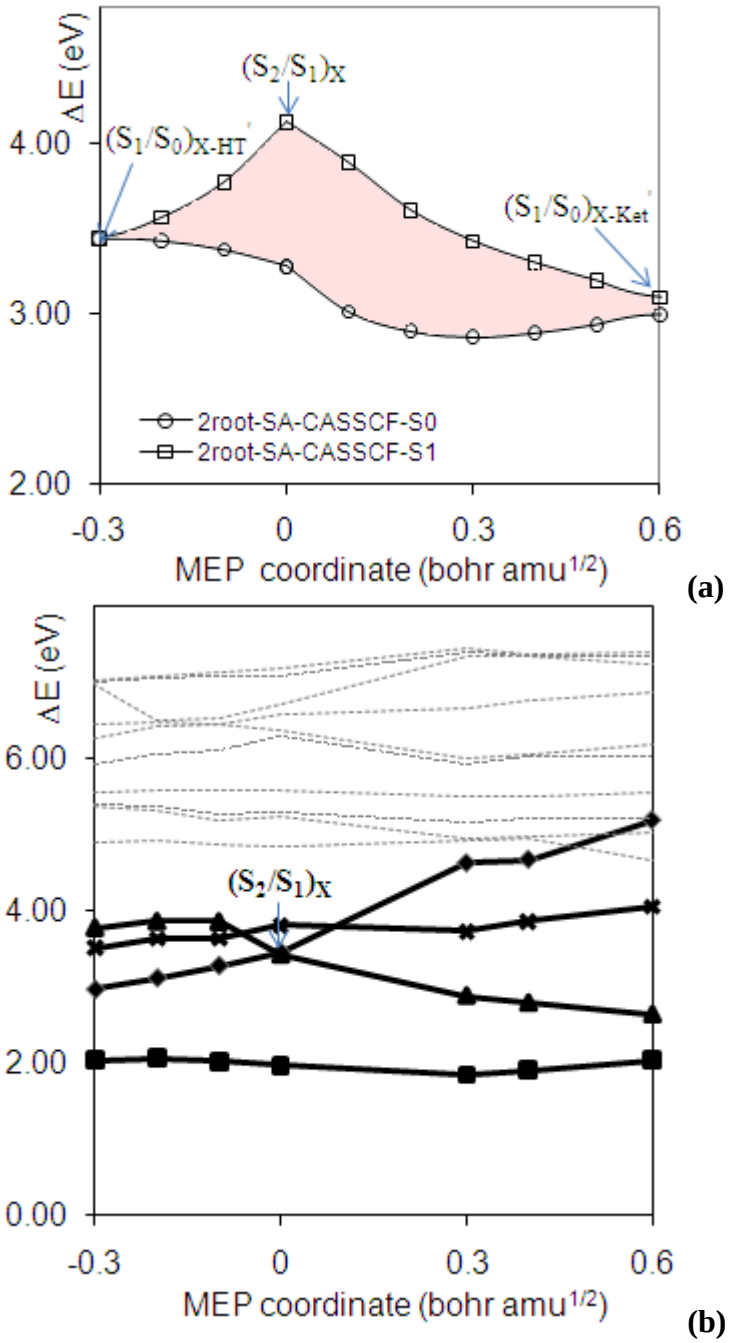

Figure SI8. (a) Combined S_1 MEP calculations from $\mathbf{(S_2/S_1)_X}$ to $\mathbf{(S_1/S_0)_{X\text{-}Ket}}$ (right direction) and $\mathbf{(S_1/S_0)_{X\text{-}HT}}$ (left direction), computed at the CASSCF level. (b) MS-CASPT2 energy profiles along the two MEPs. (♦): aldehyde ground state; (■): (n,π^*); (×): (n,π^*); (▲) ketene ground state; (--): other states.

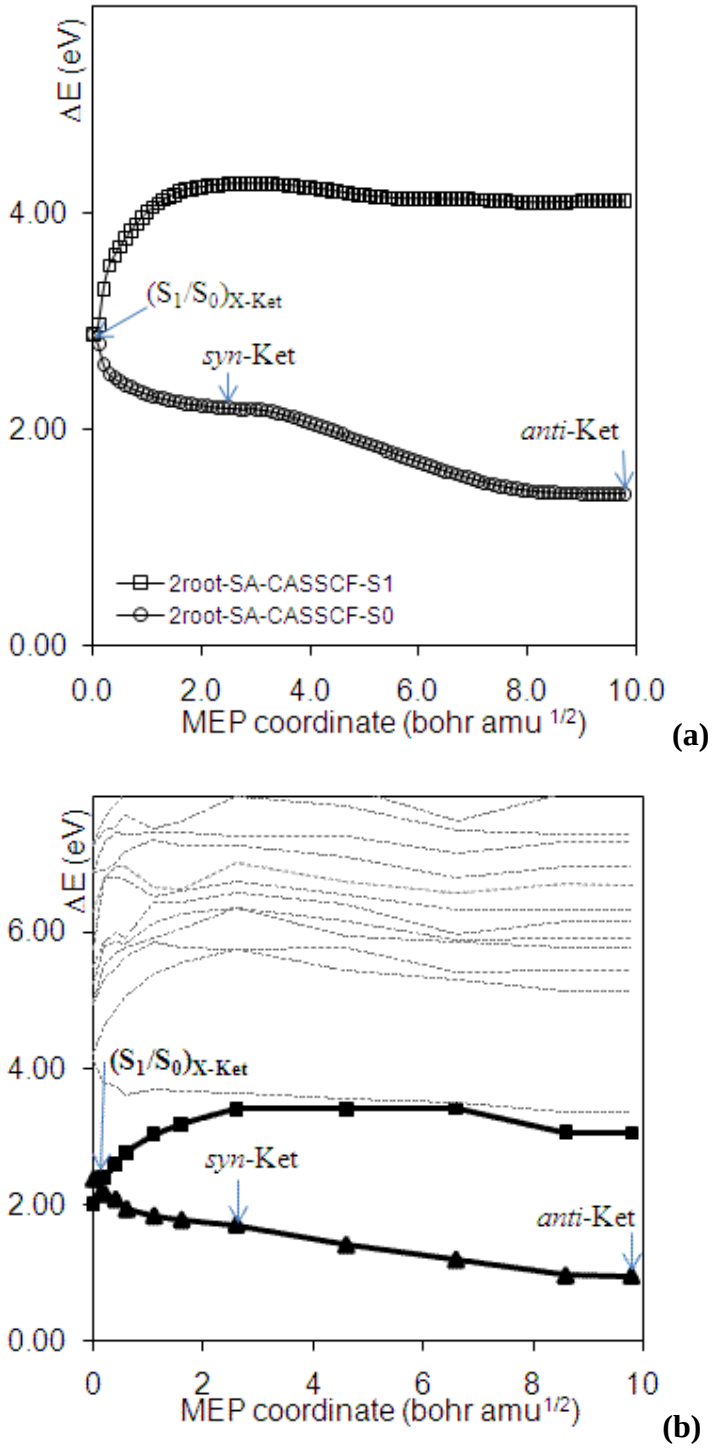

Figure SI9. (a) S_0 MEP from **$(S_1/S_0)_{X\text{-}Ket}$** to ***anti*-Ket** through ***syn*-Ket**, computed at the CASSCF level of theory. (b) MS-CASPT2 energy profiles along the MEP from **$(S_1/S_0)_{X\text{-}Ket}$** to ***anti*-Ket**. (■): (n,π^*); (▲): ketene ground state; (--): other states.

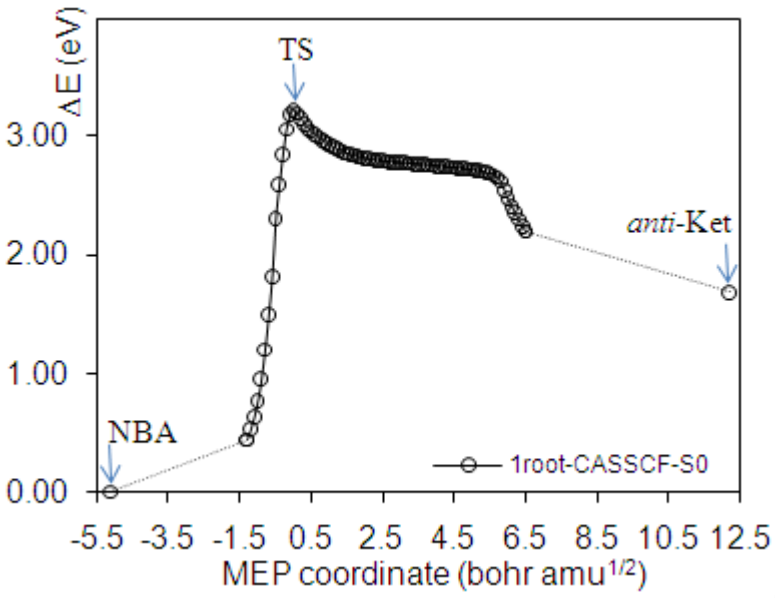

(a)

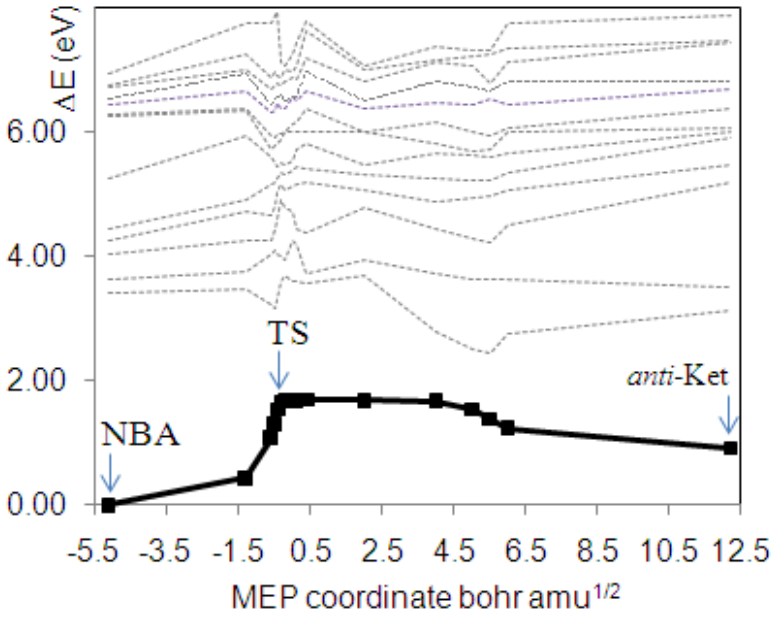

(b)

Figure SI10. (a) S_0 MEP composed by the CASSCF IRC calculations from the S_0 transition state **TS** (0.0 au of the MEP coordinate) towards **FC** and ***anti*-Ket** (left and right directions, respectively). (b) MS-CASPT2 energy profiles along the MEP from **FC** to ***anti*-Ket**. (■): S_0 (character changes from aldehyde to ketene through a (n,π^*) region); (--): other states.

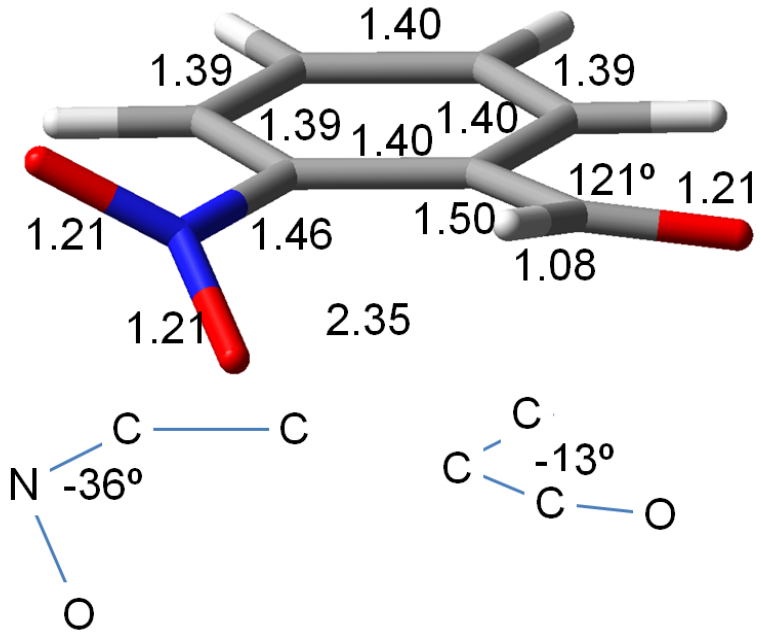

Figure SI11. Optimized S_0 NBA geometry (**FC**). Bond lengths in Å and angles in degrees.

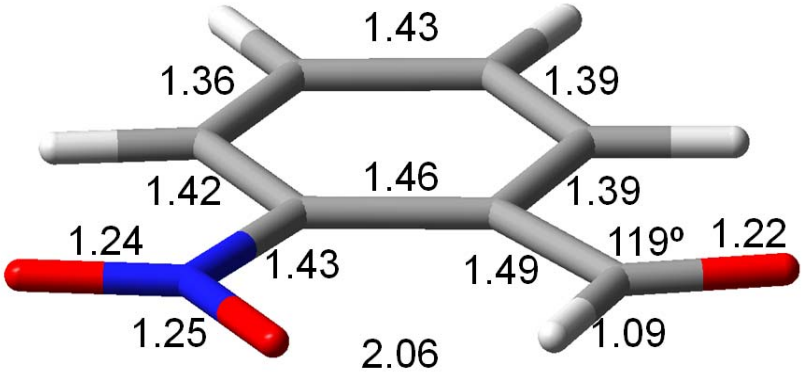

(a)

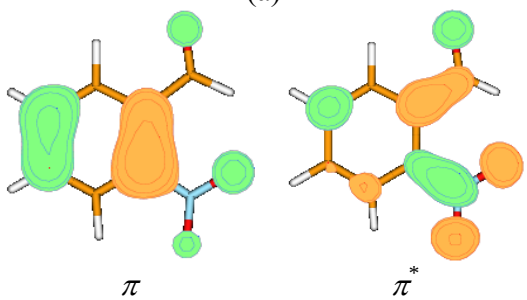

(b)

Figure SI12. (a) $(\pi,\pi^*)_{Min}$ optimized TDDFT geometry. Bond lengths in Å and angles in degrees. (b) Molecular orbitals for the (π,π^*) excitation from the CASSCF(16,13)/ANO-L wavefunction.

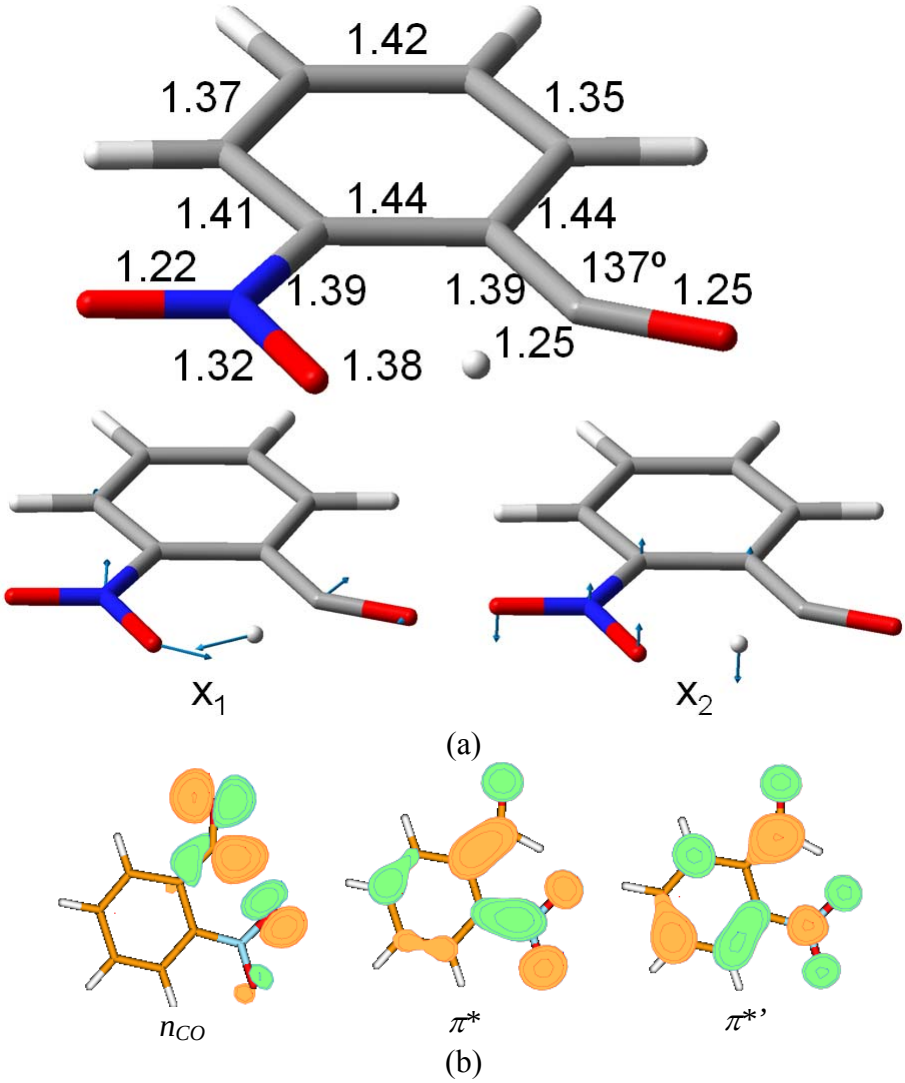

Figure SI13. (a) $(S_3/S_2)_X$ MECI geometry. x_1: gradient difference vector displacements (hydrogen transfer coupled to skeletal stretching and O-C_{10}-C_2 bond angle opening); x_2 interstate coupling vector displacements (out-of-plane motion). Bond lengths in Å and angles in degrees. (b) Molecular orbitals for the intersecting states from the CASSCF(16,13)/ANO-L wavefunction.

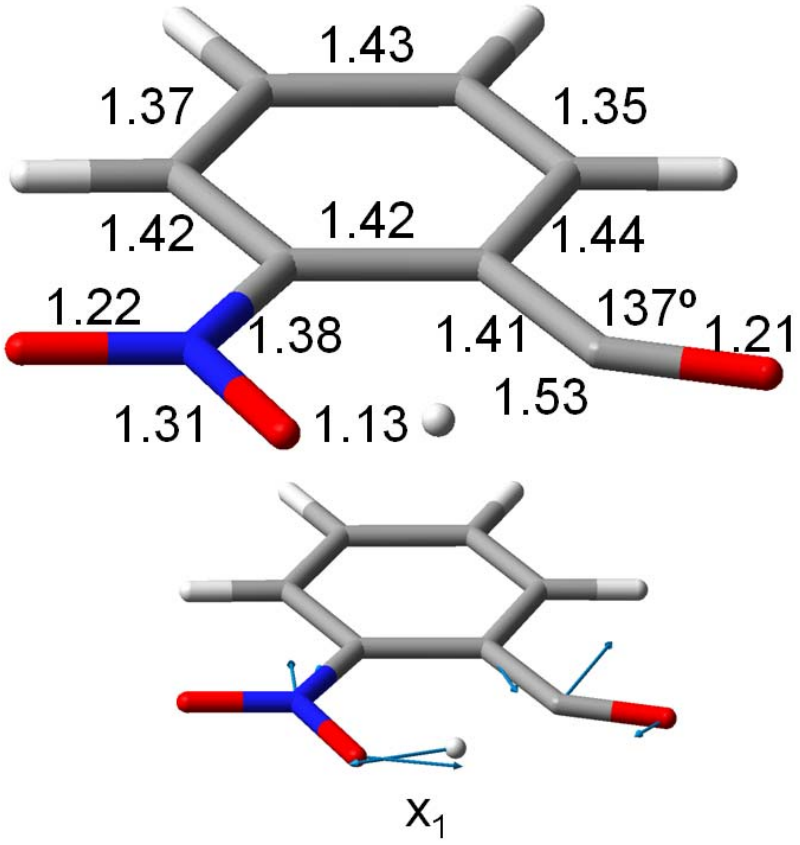

(a)

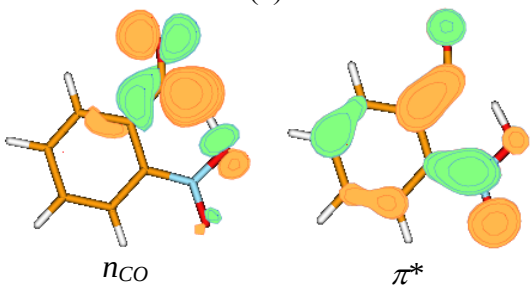

(b)

Figure SI14. (a) $(S_2/S_1)_X$ MECI geometry. x_1: gradient difference vector displacements (hydrogen transfer coupled to skeletal stretching and O-C_{10}-C_2 bond angle opening). Interstate coupling vector displacements not shown (vector has almost zero length). Bond lengths in Å and angles in degrees. (b) Molecular orbitals for the intersecting states from the CASSCF(16,13)/ANO-L wavefunction.

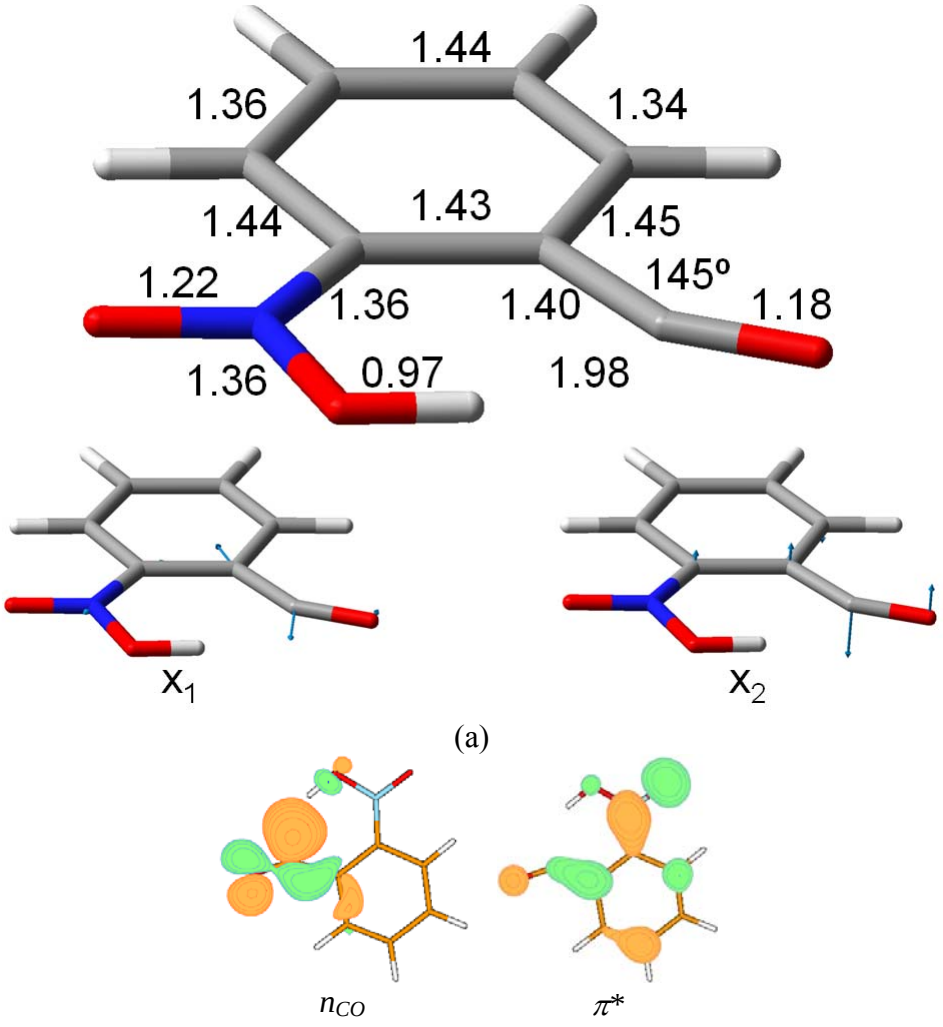

Figure SI15. (a) $(S_1/S_0)_{X\text{-}Ket}$ MECI geometry. x_1: gradient difference vector displacements (skeletal stretching coupled to O-C_{10}-C_2 bond angle opening); x_2 interstate coupling vector displacements (out-of-plane motion). Bond lengths in Å and angles in degrees. (b) Molecular orbitals for the intersecting states from the CASSCF(16,13)/ANO-L wavefunction.

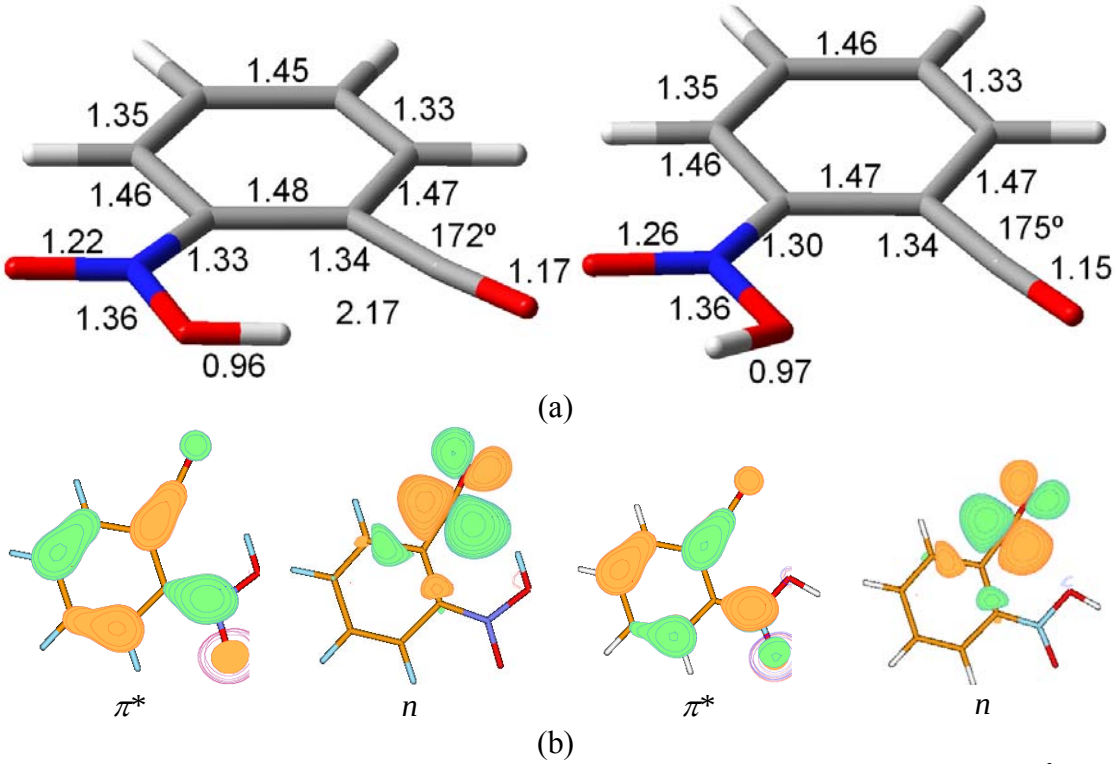

Figure SI16. (a) ***syn*-Ket** and ***anti*-Ket** optimized geometries. Bond lengths in Å and angles in degrees. (b) Molecular orbitals for both structures from the CASSCF(16,13)/ANO-L wavefunction (configuration $n^0\ \pi^{*2}$).

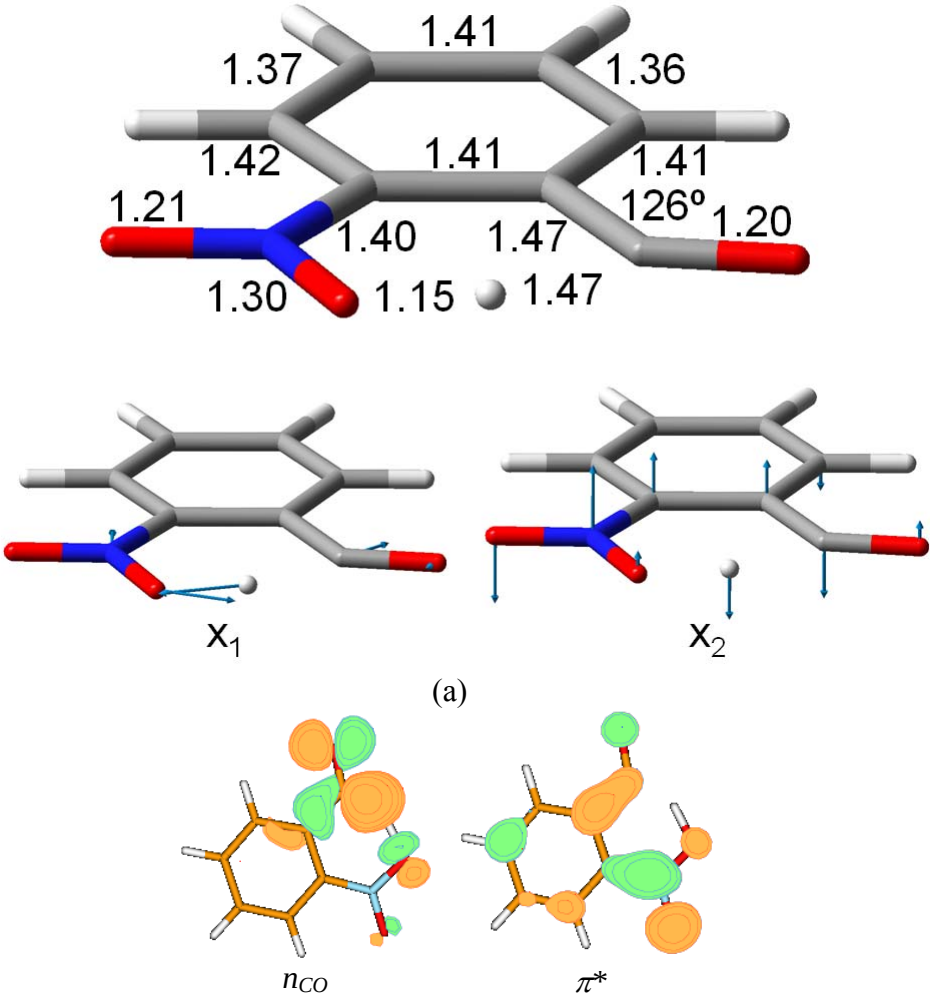

(a)

(b)

Figure SI17. (a) $(S_1/S_0)_{X\text{-}HT}$ MECI geometry. x_1: gradient difference vector displacements (hydrogen transfer coupled to skeletal stretching and O-C_{10}-C_2 bond angle opening); x_2 interstate coupling vector displacements (out-of-plane motion). Bond lengths in Å and angles in degrees. (b) Molecular orbitals for the intersecting states from the CASSCF(16,13)/ANO-L wavefunction.

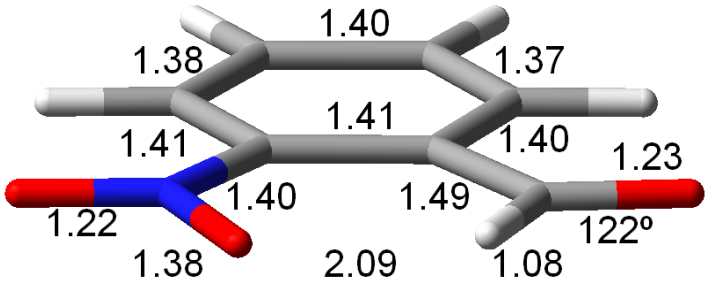

(a)

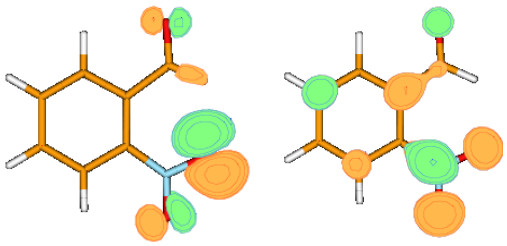

(b)

Figure SI18. (a) $(n,\pi^*)_{Min}$ optimized geometry. Bond lengths in Å and angles in degrees. (b) Molecular orbitals for the (n,π^*) state from the CASSCF(16,13)/ANO-L wavefunction.

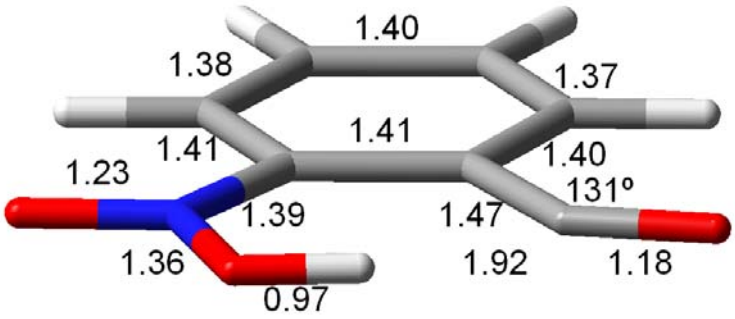

(a)

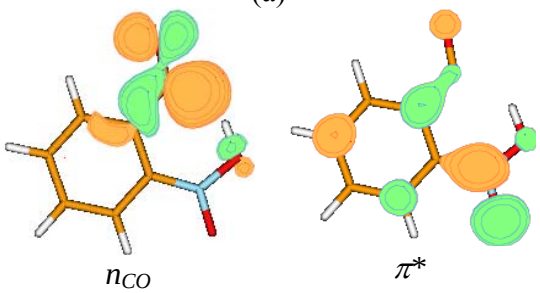

(b)

Figure SI19. (a) **Bir** optimized geometry. Bond lengths in Å and angles in degrees. (b) Singly occupied molecular orbitals from the CASSCF(16,13)/ANO-L wavefunction.

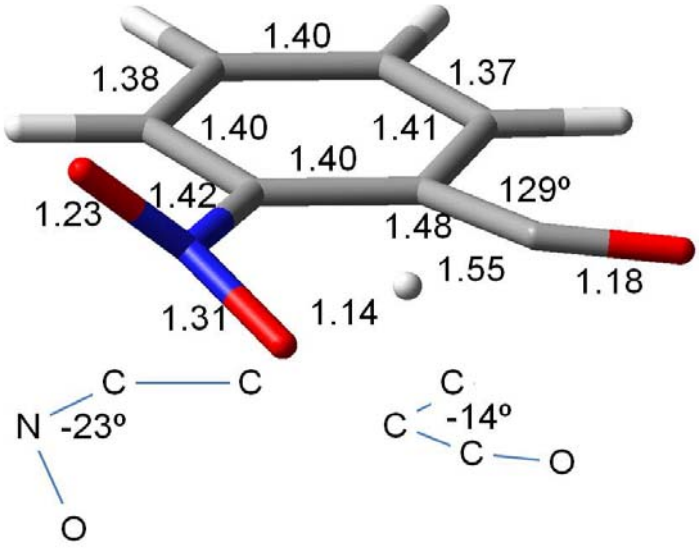

(a)

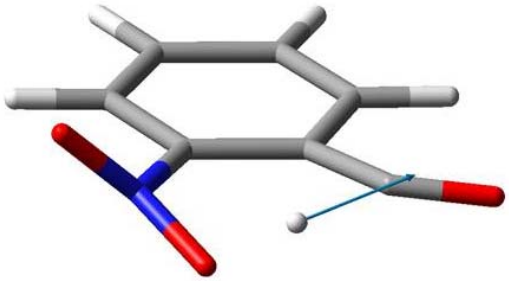

(b)

Figure SI20. (a) **TS** optimized geometry (S_0). Bond lengths in Å and angles in degrees. (b) Transition state vector associated with the imaginary frequency.

o-NBA Phototautomerization– Supporting Information - Migani et al.

Cartesian coordinates of optimized structures:

FC

C	0.0000	0.0000	0.0000
C	0.0000	0.0000	1.3954
C	1.2045	0.0000	2.0932
C	2.4347	0.0123	1.4215
C	2.4024	0.0244	0.0207
C	1.2075	0.0081	-0.6934
C	3.6830	-0.0632	2.2464
O	3.6539	0.0951	3.4420
O	4.5331	0.7767	-0.3409
O	3.6694	-0.5186	-1.7994
N	3.6307	0.0925	-0.7607
H	-0.9254	-0.0030	-0.5453
H	-0.9291	-0.0065	1.9348
H	1.2142	-0.0181	3.1654
H	1.2318	0.0119	-1.7650
H	4.6143	-0.2969	1.7492

$(\pi,\pi^*)_{Min}$

C	0.0000	0.0000	0.0000
C	0.0000	0.0000	1.4346
C	1.1968	0.0000	2.1470
C	2.4392	0.0000	1.5170
C	2.4077	0.0000	0.0587
C	1.1891	0.0000	-0.6676
C	3.6190	0.0000	2.4307
O	3.4430	0.0000	3.6363
O	4.6789	0.0000	-0.0921
O	3.4956	0.0000	-1.9654
N	3.6058	0.0000	-0.7309
H	-0.9403	0.0000	-0.5386
H	-0.9452	0.0000	1.9672
H	1.2039	0.0000	3.2316
H	1.2679	0.0000	-1.7468
H	4.6095	0.0000	1.9702

$(S_3/S_2)_X$

C	0.0059	0.0009	-0.0205
C	0.0062	-0.0030	1.4018
C	1.1586	0.0018	2.1073
C	2.4278	0.0000	1.4377
C	2.4094	-0.0030	-0.0049
C	1.1923	-0.0004	-0.7131
C	3.6598	-0.0001	2.0822
O	4.0777	0.0051	3.2552
O	4.7571	-0.0085	-0.1874
O	3.5656	0.0002	-1.9803
N	3.5726	-0.0036	-0.7638
H	-0.9211	0.0001	-0.5561
H	-0.9329	-0.0038	1.9214
H	1.1412	0.0051	3.1783
H	1.2163	0.0003	-1.7814
H	4.5213	-0.0031	1.1723

$(S_2/S_1)_X$

C	0.0137	-0.0003	-0.0154
C	0.0095	0.0014	1.4153
C	1.1652	0.0024	2.1041
C	2.4316	0.0005	1.4223
C	2.4260	-0.0012	0.0009
C	1.1902	-0.0005	-0.7085
C	3.6376	-0.0011	2.1511
O	3.9399	-0.0003	3.3231
O	4.7568	-0.0064	-0.1699
O	3.5862	0.0014	-1.9619
N	3.5855	-0.0030	-0.7466
H	-0.9174	-0.0042	-0.5477
H	-0.9290	0.0031	1.9383
H	1.1761	0.0041	3.1769
H	1.2079	-0.0048	-1.7778
H	4.5778	-0.0031	0.9442

$(S_1/S_0)_{X\text{-}Ket}$

C	1.6426	-1.9999	0.0000
C	2.5266	-0.8665	0.0000
C	2.0263	0.3759	0.0000
C	0.5986	0.6214	0.0000
C	-0.2828	-0.5087	0.0000
C	0.2920	-1.8274	0.0000
C	0.1958	1.9574	0.0000
O	0.5659	3.0828	0.0000
O	-2.3386	0.7056	0.0000
O	-2.3717	-1.4440	0.0000
N	-1.6418	-0.4613	0.0000
H	2.0524	-2.9926	0.0000
H	3.5898	-1.0220	0.0000
H	2.6735	1.2327	0.0000
H	-0.3768	-2.6620	0.0000
H	-1.7174	1.4498	0.0000

***syn*-Ket**

C	2.4259	0.7776	0.0000
C	2.5644	-0.6667	0.0001
C	1.4851	-1.4402	-0.0001
C	0.1237	-0.8872	0.0001
C	-0.0196	0.5819	0.0001
C	1.2075	1.3652	0.0000
C	-0.8207	-1.8317	0.0002
O	-1.5235	-2.7623	0.0001
O	-2.3767	0.7111	0.0004
O	-1.2229	2.5116	0.0001
N	-1.1433	1.2902	-0.0002
H	3.3064	1.3891	-0.0001
H	3.5451	-1.1026	0.0001
H	1.5777	-2.5105	-0.0001
H	1.1008	2.4291	0.0000
H	-2.3007	-0.2491	-0.0080

***anti*-Ket**

C	1.0235	-2.3620	0.0309
C	2.2444	-1.5579	0.0767
C	2.1787	-0.2314	0.0740
C	0.8896	0.4710	0.0252
C	-0.3319	-0.3371	-0.0286
C	-0.1977	-1.7876	-0.0193
C	0.9218	1.8070	0.0284
O	1.0491	2.9477	0.0381
O	-1.6054	1.5225	-0.0525
O	-2.6352	-0.4333	-0.1732
N	-1.5314	0.1653	-0.0881
H	1.1067	-3.4329	0.0382
H	3.1966	-2.0534	0.1121
H	3.0714	0.3664	0.1071
H	-1.1031	-2.3576	-0.0536
H	-2.5256	1.6788	-0.3261

$(S_1/S_0)_{X\text{-}HT}$

C	0.0086	-0.0007	-0.0064
C	0.0088	-0.0012	1.4027
C	1.1852	0.0008	2.0917
C	2.4233	0.0012	1.4143
C	2.4151	-0.0010	0.0054
C	1.1905	-0.0016	-0.7042
C	3.7141	-0.0006	2.1231
O	3.8750	0.0042	3.3091
O	4.7620	-0.0015	-0.2006
O	3.5498	-0.0035	-1.9692
N	3.5882	-0.0037	-0.7563
H	-0.9223	0.0005	-0.5421
H	-0.9242	-0.0015	1.9330
H	1.1921	0.0010	3.1641
H	1.2063	-0.0012	-1.7738
H	4.5941	-0.0034	0.9422

$(n,\pi^*)_{Min}$

C	0.0000	0.0000	0.0000
C	0.0000	0.0000	1.3979
C	1.1889	0.0000	2.0748
C	2.4289	-0.0004	1.4145
C	2.4141	-0.0005	0.0075
C	1.1941	-0.0001	-0.6936
C	3.6417	0.0002	2.2873
O	3.5515	-0.0025	3.5119
O	4.8108	0.0142	-0.2332
O	3.5828	-0.0045	-2.0273
N	3.5579	-0.0040	-0.8026
H	-0.9261	0.0003	-0.5443
H	-0.9267	0.0001	1.9382
H	1.2029	0.0002	3.1459
H	1.2123	0.0000	-1.7649

Bir

C	0.0090	-0.0013	0.0146
C	-0.0006	-0.0009	1.4152
C	1.1884	-0.0005	2.0920
C	2.4186	0.0001	1.4138
C	2.4307	-0.0011	0.0048
C	1.1997	-0.0016	-0.6856
C	3.6564	-0.0008	2.2099
O	3.8171	0.0073	3.3797
O	4.8466	-0.0022	-0.2952
O	3.5325	-0.0013	-2.0138
N	3.5772	-0.0019	-0.7876
H	-0.9178	-0.0015	-0.5294
H	-0.9318	-0.0006	1.9509
H	1.2027	0.0000	3.1659
H	1.2069	-0.0021	-1.7551
H	4.8058	-0.0112	0.6760

TS

C	0.0000	0.0000	0.0000
C	0.0000	0.0000	1.4033
C	1.1806	0.0000	2.0926
C	2.4091	0.0447	1.4073
C	2.3943	0.0507	0.0124
C	1.1920	0.0127	-0.7005
C	3.6718	-0.1124	2.1663
O	3.8487	-0.0489	3.3333
O	4.6599	0.4168	-0.0275
O	3.7614	-0.7993	-1.6221
N	3.6198	-0.0020	-0.6971
H	-0.9313	-0.0125	-0.5353
H	-0.9332	0.0008	1.9360
H	1.1936	-0.0196	3.1665
H	1.2167	-0.0109	-1.7722
H	4.6601	-0.1207	0.9741